

Giant and Gate-tunable Spin-Galvanic Effect in Graphene-Topological insulator van der Waals Heterostructures at Room Temperature

Dmitrii Khokhriakov¹, Anamul Md. Hoque¹, Bogdan Karpiak¹, Saroj P. Dash^{1*}

¹*Department of Microtechnology and Nanoscience, Chalmers University of Technology, SE-41296, Göteborg, Sweden*

Abstract

Unique electronic spin textures in topological states of matter are promising for emerging spin-orbit driven memory and logic technologies. However, there are several challenges related to the enhancement of their performance, electrical gate-tunability, interference from trivial bulk states, and heterostructure interfaces. We address these challenges by integrating two-dimensional graphene with a three-dimensional topological insulator (TI) in a van der Waals heterostructure to take advantage of their remarkable spintronic properties and engineer strong proximity-induced spin-charge conversion phenomena. In these heterostructures, we experimentally demonstrate a giant spin-galvanic effect at room temperature due to efficient conversion of a nonequilibrium spin polarization into a transverse charge current with signal amplitude orders of magnitude larger than that observed in conventional materials. Importantly, using a gate voltage we achieve a strong electric field tunability of the spin-galvanic signal and its sign-switch functionality, which can be attributed to the proximity-induced Rashba-Edelstein effect in graphene. These findings provide a new and efficient route for realizing all-electrical and gate-tunable spin-orbit technology using TIs and graphene in heterostructures which can greatly enhance the performance and reduce power dissipation in spintronic circuits.

Keywords: Graphene, Topological Insulator, van der Waals heterostructures, Proximity effect, Spin Hall effect, Spin-Galvanic effect, Rashba-Edelstein effect.

Corresponding author: saroj.dash@chalmers.se

Main

Spin-based memory, oscillators and logic devices operating at high speed and at low power are promising for future artificial intelligence and information technology¹⁻³. In these device architectures, spin-polarized currents are used to exert a spin-orbit torque (SOT) on an adjacent magnetic layer⁴, enabling a manipulation, persistent oscillation and even switching of the magnetization^{5,6}. The key to these technologies so far is the use of heavy metals, semiconductors and heterostructure interfaces of metals and oxides utilizing their strong spin-orbit interaction (SOI) and broken inversion symmetry, which allow for a charge-current-induced spin accumulation via spin Hall and Rashba-Edelstein effects⁷. Recently, such charge-spin conversion process and its inverse phenomenon were investigated in semimetals⁸, transition metal dichalcogenides (TMDs)⁹, and graphene/TMD heterostructures¹⁰⁻¹². However, so far, the achieved efficiency of the spin-charge conversion effect is limited and theoretically predicted gate-induced sign switching of spin signals has not been demonstrated¹³.

To further enhance the efficiency of magnetization dynamics and to reduce the power consumption of charge-spin conversion beyond the capacity of conventional materials, topological insulators (TIs) can be introduced¹⁴. This allows to take advantage of their topologically protected Dirac surface states with a distinct spin-momentum locking (SML) feature which gives rise to a spontaneous electron spin polarization by application of an electric field. Recently, electric detection of SML states¹⁵⁻¹⁹ and large charge-spin conversion with an efficient SOT²⁰⁻²² have been demonstrated up to room temperature using TIs in contact with ferromagnetic materials. In particular, stronger charge-spin conversion efficiency of highly-conducting p-type TIs has been revealed^{1,23}. However, there are several challenges related to the electrical tunability of charge-spin conversion signals in TIs, their unintentional doping issues²⁴ and possible destruction of topological surface states in contact with ferromagnets at the interface²⁵.

Here, we introduce an atomically-thin graphene (Gr) layer in van der Waals heterostructures with a p-type TI ((Bi_{0.15}Sb_{0.85})₂Te₃) to experimentally demonstrate a giant spin-galvanic effect (SGE) at room temperature due to an efficient spin-charge conversion process. The gate-tuning of SGE signal and its sign-switch functionality, which cannot be achieved in these materials individually, demonstrate the all-electrical operation of a hybrid spintronic device. Our comprehensive measurements and control experiments reveal that the main contribution to the observed SGE signal originates from the Rashba-Edelstein effect in the Gr-TI heterostructure due to the proximity-induced SOI in graphene.

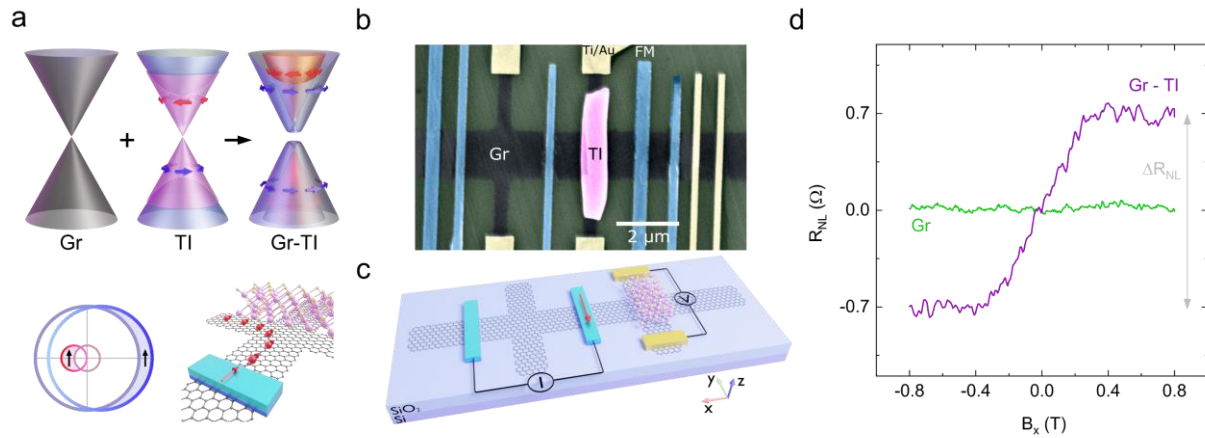


Figure 1. Giant spin-galvanic effect in the graphene-topological insulator heterostructure at room temperature. **a**, Schematics of band structures of pristine graphene (Gr), topological insulator (TI) and Rashba spin-split band in graphene due to proximity induced spin-orbit interaction (SOI) in a Gr-TI heterostructure. The bottom panels show the shift of Rashba spin-split Fermi circles in k -space due to injection of spin polarized current into the Gr-TI heterostructure region, and the resulting spin-galvanic effect (SGE). **b**, Colored scanning electron microscopy picture of a representative hybrid device consisting of a Hall bar structure with Gr-TI heterostructure and pristine graphene channels with TiO_2/Co ferromagnetic tunnel contacts (FM) and reference nonmagnetic (Ti/Au) contacts on the graphene. **c**, A schematic of the device with a non-local measurement geometry used for probing the SGE in the Gr-TI heterostructure. A spin current is injected from a FM contact into the Gr-TI heterostructure region and the SGE is detected as a voltage signal across the Hall cross by nonmagnetic contacts. **d**, The SGE signal R_{NL} measured in the Gr-TI heterostructure (purple color data) with a magnetic field sweep in the x -direction (B_x) with an application of a spin injection bias current of $I = -150 \mu\text{A}$ and a gate voltage $V_g = 40 \text{V}$ at room temperature. A linear background is subtracted from the data as shown in Fig. S10. A control experiment with voltage measured across a pristine graphene Hall cross (green color data) in a mirrored SGE measurement geometry shows a null signal.

The introduction of a graphene layer in a van der Waals heterostructure with a TI is theoretically predicted to preserve the topological bands of TIs²⁶ while also introducing a strong SOI in the graphene^{27–30}. Such proximity-induced SOI can result in Rashba spin-splitting of the graphene bands (schematically shown in Fig. 1a) and can give rise to a spin-galvanic effect due to an efficient spin-charge conversion. The SGE in such a system can be probed by injecting a non-equilibrium spin polarization into the Gr-TI heterostructure region, which can lead to a shift of the Fermi circles in k -space. This results in spin-polarized carriers acquiring a net transverse momentum in real space and thus creating charge current in the heterostructure region (bottom panels of Fig. 1a).

To investigate spin-charge conversion in a hybrid Gr-TI system, we fabricated a device (Fig. 1b) consisting of a Hall-bar-shaped CVD graphene³¹ with a flake of p-type TI $(\text{Bi}_{0.15}\text{Sb}_{0.85})_2\text{Te}_3$ placed on top of a Hall cross (see Supplementary Fig. S1-3 for device characterization). Single crystal

flakes of the TI were exfoliated and transferred onto the graphene inside a glovebox in a controlled environment to achieve clean van der Waals interfaces. The graphene was subsequently patterned and contacted by ferromagnetic (TiO₂/Co with contact resistance of 5-10 k Ω) and reference nonmagnetic (Ti/Au with contact resistance of around 1 k Ω) electrodes in a multi-step electron beam lithography process (see Methods). Basic spin transport characterization of pristine graphene and Gr-TI heterostructure regions was performed using conventional spin valve and Hanle spin precession measurements, as described in the Supplementary note 1 and Supplementary Fig. S4. These studies show a good spin transport quality of our graphene, with spin lifetime $\tau_s = 327$ ps and spin diffusion length $\lambda_s = 3$ μm . On the other hand, a strong decrease of the spin signal amplitude is observed in the Gr-TI heterostructure channel, indicating the presence of a significant SOI.

We utilized such Gr-TI heterostructures to demonstrate a giant spin-galvanic effect that allows converting spin information into its charge representation. In our non-local Hall measurement geometry (Fig. 1c), a spin-polarized current I is injected from a ferromagnetic (FM) contact into the graphene channel creating non-equilibrium spin accumulation, which diffuses towards the Gr-TI heterostructure as pure spin current. Consequently, a transverse charge current is created via the SGE in the Gr-TI heterostructure, which is measured using nonmagnetic contacts across the Gr-TI Hall cross. The magnetization direction of injector FM is used to control the orientation of injected spin polarization. With an application of an external magnetic field along the x-direction (B_x), the injected spins experience precession in the y-z plane while the injector FM magnetization \vec{M} rotates in the x-y plane and aligns with the field in the x-direction. As a consequence of the FM magnetization rotation, the measured signal $\Delta R_{NL} = \Delta V_{NL}/I$ increases or decreases anti-symmetrically at low fields and saturates as the rotation completes at $B_{\text{sat}} \approx \pm 0.4$ T, as shown in Fig. 1d. The value of B_{sat} was confirmed with spin precession experiments (Fig. S4d) and anisotropic magnetoresistance measurements (Fig. S5). We obtained a giant SGE signal magnitude of $\Delta R_{NL} = 1.4$ Ω , which is much larger than values found in trivial materials and heterostructures^{11,12}. Similar results were also reproducibly obtained at room temperature in another device fabricated on a different chip, as shown in Fig. S6.

Control experiments performed in the pristine graphene part of the Hall-bar structure result in a null signal (the green curve in Fig. 1d, Supplementary Information Fig. S7), providing further proof of the origin of observed SGE to be only from the Gr-TI heterostructure regions. To rule out any other charge-based contributions to the observed SGE, we performed additional control experiments in Gr-TI Hall bar devices having only nonmagnetic contacts, as shown in Supplementary Fig. S8. These measurements confirm the absence of SGE-like signals in the devices without a spin-polarized current injection into the Gr-TI heterostructure region, further supporting the spin origin of the observed SGE signal.

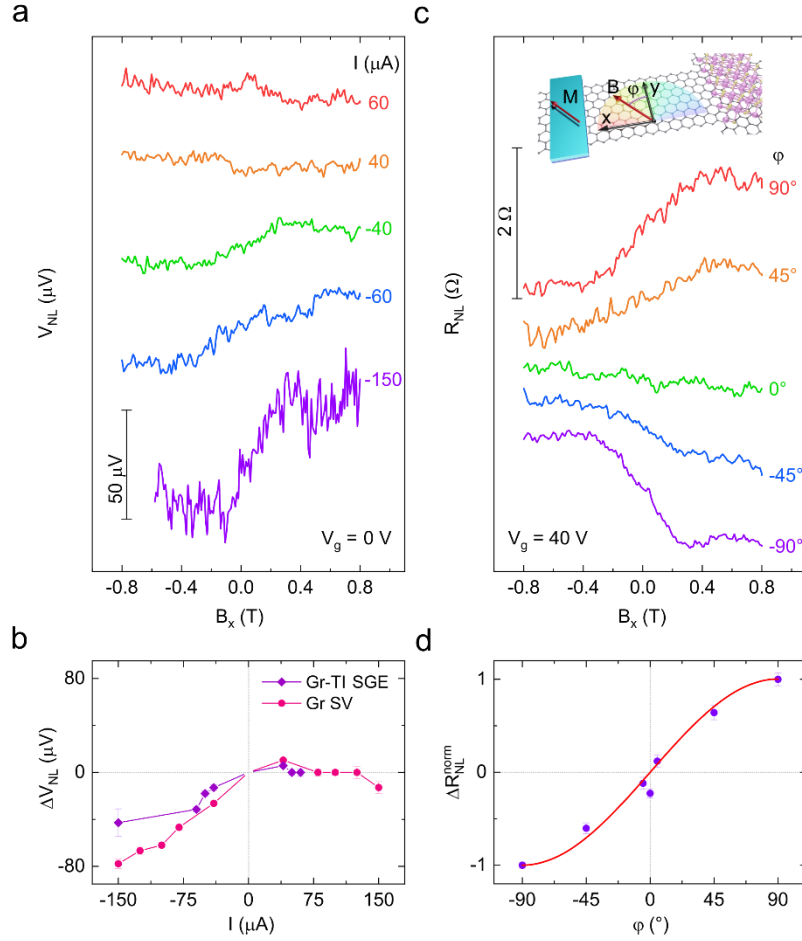


Figure 2. Bias and angle dependence of the spin-galvanic effect in the graphene-topological insulator heterostructure. **a**, SGE signals measured at various applied spin injection bias currents I with $V_g = 0$ V. **b**, The nonlocal voltage amplitude for the SGE and SV signals versus the bias current. Both signals are obtained with the same injector FM contact. Solid lines are guides to the eye. **c**, SGE signals measured at various angles ϕ with $I = -150$ μA and $V_g = 40$ V. The inset shows the utilized coordinate axes with the angle ϕ between the magnetic field B and the y -axis in the graphene plane. The angle $\phi = \pm 90^\circ$ corresponds to the positive B field applied in $\pm x$ directions. A linear background was subtracted from all the curves, as shown in Fig. S10. **d**, Normalized amplitude of the SGE signal ΔR_{NL} as a function of angle ϕ with the red line representing a $\sin(\phi)$ function. All the measurements are performed at room temperature.

To gain an insight into the behavior of SGE signal with varying spin injection bias current I applied to the FM contact, we performed systematic measurements as shown in Fig. 2a. Here the $+I$ corresponds to spin injection and $-I$ corresponds to spin extraction regimes, which are expected to create spin accumulation with opposite polarizations and hence an opposite sign of SGE signals. However, we observed a very asymmetric bias dependence of the SGE signal, where a strong signal was observed for $-I$ and a diminished signal in the $+I$ regime. To understand this behavior, we compare the SGE signal with the standard spin valve measurements (SV) using the same FM spin injector contact for both cases, tracking its spin injection and extraction characteristics with bias current (see Supplementary Fig. S9 for details). Figure 2b summarizes

these measurements, showing a strong correlation in the bias dependence trends for the SGE and SV signals. These measurements confirm the common spin origin of SGE and SV signals, as their magnitude is directly proportional to the spin injection efficiency of the FM contact.

To further investigate the origin of the signal, we performed measurements with a varying angle between the external magnetic field and the easy magnetization direction of the FM injector in the graphene plane, as shown in Fig. 2c. The magnetization direction of FM electrodes is controlled by the magnetic field, and such angle dependence allows us to study the spin-charge conversion for spins oriented in different directions. The 90° data correspond to the signal obtained with magnetic field oriented in the $+x$ direction (B_x), probing the sign and magnitude of R_{NL} for spins oriented in the $+x$ direction. Similarly, -90° corresponds to the magnetic field and spin polarization pointing in the $-x$ direction, resulting in a R_{NL} of similar magnitude but with an opposite sign. The absence of a signal at $\varphi = 0^\circ$ indicates that the spin polarization along the y -axis does not create any charge current in the same y -direction. Similar behavior was reproducibly observed in the device 2, as shown in Fig. S10b. The normalized amplitude of SGE signals ΔR_{NL} as a function of angle φ follows the $\sin(\varphi)$ curve (Fig. 2d), as expected for the antisymmetric SGE signal. Overall, the angle-dependent measurements of SGE revealed its strong dependence on the orientation of the magnetic field conforming to the expected $\sin(\varphi)$ trend and proving the momentum \vec{k} and spin \vec{s} orthogonality of spin-charge conversion mechanism⁷.

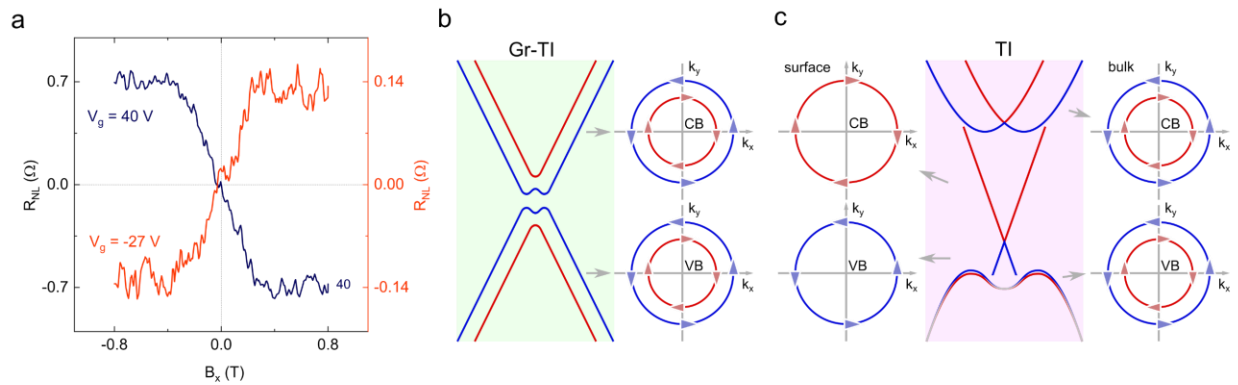


Figure 3. Gate-controlled sign change of spin-galvanic signal in the graphene-topological insulator heterostructure. **a**, SGE signals measured with Fermi level tuned to the conduction ($V_g = 40$ V) and valence ($V_g = -27$ V) bands of proximitized graphene at room temperature. A linear background is subtracted from the data (see Fig. S10). **b**, A schematic band structure of Gr in proximity to a TI with indicated spin textures of the Rashba spin-split bands in electron- and hole-doped regimes. Colors represent the helicity of bands. **c**, A schematic of the simplified band structure of TI surface and Rashba-split bulk states with corresponding Fermi contours indicating their spin texture.

One of the most essential functionalities of spintronic devices is the possibility to control the spin information by a gate electric field. An application of the back-gate voltage V_g in our device is expected to mainly tune the Fermi level (E_f) in the proximitized graphene with a partial tuning of TI Dirac surface states at the interface, whereas the bulk bands of TI may be gate-insensitive due to their strong p-type doping. Figure 3a shows the SGE signals measured at two representative

gate voltages, corresponding to the E_f tuned to the conduction ($V_g = 40$ V) and valence bands ($V_g = -27$ V). A clear change of the signal sign is observed, demonstrating gate-tunability and efficient switching functionality of SGE in the Gr-TI heterostructures.

To understand the microscopic mechanism of the observed SGE signal and explain its gate-dependent sign change behavior, we consider several possible sources of spin-charge conversion in our Gr-TI heterostructures. As predicted by theoretical investigations, the proximity-induced SOI in graphene can give rise to Rashba spin-splitting of the graphene bands with opening of a bandgap (\sim few meV) and a spin texture with the same spin winding direction in low-energy conduction and valence bands²⁹ (Fig. 3b), which can give rise to proximity-induced inverse Rashba-Edelstein effect (IREE) and inverse spin Hall effect (ISHE) in graphene. In addition, we discuss possible contributions from the inverse Edelstein effect (IEE) in TI surface states and inverse Rashba-Edelstein effect and inverse spin Hall effect in TI bulk bands.

First, we consider the (I)REE in graphene, where the proximity-induced spin texture can result in the conversion of spin density into a charge current in the orthogonal direction to the spin orientation. Since we do not observe any significant features related to the out-of-plane component of the spin in our data at $B < B_{\text{sat}}$, we consider only the in-plane Rashba spin texture in our analysis^{27,29}. In such Rashba system, the change in the sign of IREE signal is expected when the E_f is tuned across the charge neutrality point (CNP) of a Gr-TI heterostructure, since electrons and holes with the same spin acquire the momentum in the same direction, which creates the charge current of opposite signs depending on the majority carrier type due to the negative (positive) electric charge of electrons (holes).

We can rule out a contribution from the proximity-induced ISHE in graphene. An ISHE describes how a spin current \vec{I}_s in a material can create a charge current \vec{I}_c that is perpendicular to both \vec{I}_s and spin orientation \vec{s} . In graphene, due to its 2D structure, this effect can only be observed when the spin \vec{s} is pointing out-of-plane along z , while both \vec{I}_s and \vec{I}_c are in-plane and perpendicular to each other. In our measurement geometry, spin polarization along z can only occur at moderate magnetic fields ($0 < B < B_{\text{sat}}$) due to spin precession, whereas at $B > B_{\text{sat}}$ the spins are polarized along x and do not experience precession, thus no ISHE signal is expected. Since our signal is clearly non-zero at $B > B_{\text{sat}}$, we can exclude the proximity-induced ISHE in graphene. Besides, the same reasoning can be utilized to rule out thermal effects like the inverse spin Nernst effect³², since it has the same symmetry as the ISHE.

Next, we consider possible contributions from spin textures in spin-polarized Dirac surface states and Rashba spin-split bulk bands of TIs, which have opposite spin winding in the conduction band and an asymmetric convoluted dispersion near the valence band edge^{15,18,33–35}. Fig. 3c shows a simplified schematic of the TI band structure, allowing to assess relative contributions of different channels. First, as the TI surface spin texture is opposite for holes and electrons, it is not expected to produce a sign change in the measurement^{15,18}. Although the Rashba bulk states of the TI can yield opposite signs of the SGE in the conduction and valence bands, in our experimental conditions the E_f is not expected to reach the bulk conduction band due to the high hole doping of the TI and, therefore, we can rule out these states as the origin of observed sign change.

Similarly, the ISHE in the TI bulk bands is not expected to contribute to the sign change, since we are not able to change the carrier type in these bands by the gate voltage. This leaves the IREE in proximitized graphene as the only mechanism that can be responsible for the observed sign change of the SGE signal.

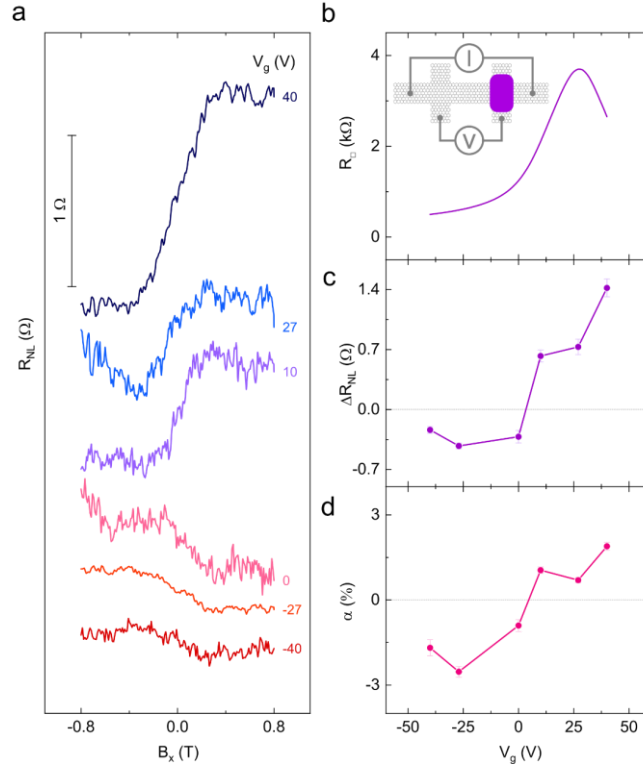


Figure 4. Gate tunability of the spin-galvanic signal in the graphene-topological insulator heterostructure. **a**, SGE signals measured at various applied back gate voltages with $I = -150 \mu\text{A}$. **b**, The gate dependence of graphene channel sheet resistance, showing a CNP at $V_g = 27 \text{ V}$. The inset shows the measurement geometry. **c**, The magnitude of SGE signal ΔR_{NL} as a function of gate voltage. The solid line is a guide to the eye. **d**, The extracted Rashba-Edelstein effect efficiency parameter α at various gate voltages.

To further assess the sign change of spin-charge conversion signal in our devices, we performed detailed measurements at various gate voltages as shown in Fig. 4a. The V_g dependence of channel sheet resistance R_s and SGE magnitude ΔR_{NL} are plotted in Fig. 4b-c, showing a sign change point of the signal (V_0) between 0 and 10 V, which seems to deviate from the CNP of graphene ($V_{\text{CNP}} = 27 \text{ V}$). However, note that the R_s measurement (see the geometry in the inset of Fig. 4b) includes contributions from the graphene channel (with $L = 4.8 \mu\text{m}$) and the Gr-TI heterostructure ($L = 1 \mu\text{m}$), while, individually, they can have different charge neutrality points due to the charge transfer between graphene and TI. This can result in a local CNP in the Gr-TI heterostructure region that differs from that of the uncovered graphene, while coinciding with the sign change point of the SGE signal. Another possible source of such deviation can be due to the influence of the TI states, depending on the relative orientation of their spin texture and the sign of produced charge current. We consider several cases with varying degree of E_f -tunability in the

TI (see Supplementary note 3), however, we could expect a possible shifting of V_0 only towards the conduction band ($V_g > V_{\text{CNP}}$), whereas, experimentally, the sign change happens on the valence band side ($V_g < V_{\text{CNP}}$). As in our device geometry the injector and detector electrodes are placed on the graphene which has a charge transport barrier to the TI with the zero-bias interface resistance of a few k Ω (see Supplementary Fig. S3), we expect the main contribution to the measured SGE signal to originate from the IREE in the proximitized graphene in a van der Waals heterostructure with the TI.

We estimate the efficiency of spin-charge conversion process assuming that the SGE in our devices is fully governed by the IREE in the Gr-TI heterostructure, which is described by¹¹

$$\Delta R_{\text{IREE}} = \frac{\alpha P_i R_{\square} \lambda_s}{W_H} \left(e^{-\frac{L}{\lambda_s}} - e^{-\frac{L+W_H}{\lambda_s}} \right)$$

, where α is the IREE efficiency parameter, P_i is polarization of the injector contact, R_{\square} is graphene sheet resistance, λ_s is spin diffusion length in the Gr-TI hybrid structure, W_H is the width of the Hall bar arms and L is the distance between the injector and the Hall cross (see Supplementary note 4 for details). The calculated efficiency and its gate tunability are plotted in Fig. 4d, with $|\alpha|$ reaching 2.5% in the device 1. In the device 2 we obtain α as large as 4.8% (see Supplementary note 4), exceeding values seen in Gr-TMD heterostructures^{11,12}. Such large spin-charge conversion efficiency and its gate tunability in the Gr-TI heterostructures mitigate the lack of field effect in the strongly doped TIs and, therefore, can be highly relevant for applications in all-electrical spin-orbit technologies.

In conclusion, we integrate the 3D topological insulator and 2D graphene in van der Waals heterostructures to demonstrate a giant spin-galvanic effect, allowing an efficient conversion between spin- and charge-based information at room temperature. Importantly, we observe a strong tunability and a sign change of the spin-galvanic signal by the gate electric field, which most likely originate from the proximity-induced Rashba-Edelstein effect in the graphene. By probing an energy-dependent spin texture and chirality of the hybrid bands with Rashba spin-splitting, we provide valuable insights into the physics of proximity-induced SOI in graphene-TI heterostructures. The observed giant and gate-tunable spin-charge conversion effect can offer unique advantages for faster and low-power spin-orbit torque-based logic and memory applications^{1,6}. These results open a new route for the design of highly tunable spin-orbit phenomena with novel spin textures based on van der Waals heterostructures, which can become an essential building block in functional spintronic circuits, artificial intelligence³, and topological quantum technology³⁶.

Note: After the preparation of this manuscript, recent preprints appeared on graphene/TMD heterostructures, including semiconducting WS₂ [ref 37] and semimetallic TaS₂ [ref 38] and 1T' MoTe₂ [ref 39]. In contrast, our results show for the first time a giant spin-charge conversion effect in graphene-topological insulator heterostructures with gate-tunable functionality, resolving the challenges that were preventing the utilization of TIs in practical spintronic devices.

References

1. Manipatruni, S. *et al.* Scalable energy-efficient magnetoelectric spin-orbit logic. *Nature* **565**, 35–42 (2019).
2. Brataas, A. & Hals, K. M. D. Spin-orbit torques in action. *Nat. Nanotechnol.* **9**, 86 (2014).
3. Romera, M. *et al.* Vowel recognition with four coupled spin-torque nano-oscillators. *Nature* **563**, 230–234 (2018).
4. Miron, I. M. *et al.* Perpendicular switching of a single ferromagnetic layer induced by in-plane current injection. *Nature* **476**, 189–193 (2011).
5. Awad, A. A. *et al.* Long-range mutual synchronization of spin Hall nano-oscillators. *Nat. Phys.* **13**, 292 (2016).
6. Manchon, A. *et al.* Current-induced spin-orbit torques in ferromagnetic and antiferromagnetic systems. *Rev. Mod. Phys.* **91**, 35004 (2019).
7. Sinova, J., Valenzuela, S. O., Wunderlich, J., Back, C. H. & Jungwirth, T. Spin Hall effects. *Rev. Mod. Phys.* **87**, 1213–1260 (2015).
8. Zhao, B. *et al.* Observation of Spin Hall Effect in Semimetal WTe₂. *arXiv Prepr. arXiv1812.02113* (2018).
9. Shao, Q. *et al.* Strong Rashba-Edelstein Effect-Induced Spin-Orbit Torques in Monolayer Transition Metal Dichalcogenide/Ferromagnet Bilayers. *Nano Lett.* **16**, 7514–7520 (2016).
10. Offidani, M., Milletari, M., Raimondi, R. & Ferreira, A. Optimal Charge-to-Spin Conversion in Graphene on Transition-Metal Dichalcogenides. *Phys. Rev. Lett.* **119**, (2017).
11. Safeer, C. K. *et al.* Room-Temperature Spin Hall Effect in Graphene/MoS₂ van der Waals Heterostructures. *Nano Lett.* **19**, 1074–1082 (2019).
12. Ghiasi, T. S., Kaverzin, A. A., Blah, P. J. & van Wees, B. J. Charge-to-Spin Conversion by the Rashba-Edelstein Effect in Two-Dimensional van der Waals Heterostructures up to Room Temperature. *Nano Lett.* **19**, 5959–5966 (2019).
13. Garcia, J. H., Vila, M., Cummings, A. W. & Roche, S. Spin transport in graphene/transition metal dichalcogenide heterostructures. *Chem. Soc. Rev.* **47**, 3359–3379 (2018).
14. Hasan, M. Z. & Kane, C. L. Colloquium: Topological insulators. *Rev. Mod. Phys.* **82**, 3045–3067 (2010).
15. Li, C. H. *et al.* Electrical detection of charge-current-induced spin polarization due to spin-momentum locking in Bi₂Se₃. *Nat. Nanotechnol.* **9**, 218 (2014).
16. Dankert, A., Geurs, J., Kamalakar, M. V., Charpentier, S. & Dash, S. P. Room Temperature Electrical Detection of Spin Polarized Currents in Topological Insulators. *Nano Lett.* **15**, 7976–7981 (2015).
17. Dankert, A. *et al.* Origin and evolution of surface spin current in topological insulators. *Phys. Rev. B* **97**, 125414 (2018).
18. Li, C. H., van 't Erve, O. M. J., Li, Y. Y., Li, L. & Jonker, B. T. Electrical Detection of the Helical Spin Texture in a p-type Topological Insulator Sb₂Te₃. *Sci. Rep.* **6**, 29533 (2016).
19. Voerman, J. A., Li, C., Huang, Y. & Brinkman, A. Spin-Momentum Locking in the Gate Tunable Topological Insulator BiSbTeSe₂ in Non-Local Transport Measurements. *Adv. Electron. Mater.* **0**, 1900334 (2019).
20. Mellnik, A. R. *et al.* Spin-transfer torque generated by a topological insulator. *Nature* **511**, 449 (2014).
21. Khang, N. H. D., Ueda, Y. & Hai, P. N. A conductive topological insulator with large spin Hall effect for ultralow power spin-orbit torque switching. *Nat. Mater.* **17**, 808–813 (2018).
22. DC, M. *et al.* Room-temperature high spin-orbit torque due to quantum confinement in sputtered Bi_xSe_(1-x) films. *Nat. Mater.* **17**, 800–807 (2018).
23. Kondou, K. *et al.* Fermi-level-dependent charge-to-spin current conversion by Dirac surface states of topological insulators. *Nat. Phys.* **12**, 1027 (2016).
24. Ando, Y. Topological Insulator Materials. *J. Phys. Soc. Japan* **82**, 102001 (2013).
25. Pai, C.-F. Switching by topological insulators. *Nat. Mater.* **17**, 755–757 (2018).
26. Rodriguez-Vega, M., Schwiete, G., Sinova, J. & Rossi, E. Giant Edelstein effect in topological-insulator-graphene heterostructures. *Phys. Rev. B* **96**, (2017).
27. Song, K. *et al.* Spin Proximity Effects in Graphene/Topological Insulator Heterostructures. *Nano Lett.* (2018). doi:10.1021/acs.nanolett.7b05482
28. Khokhriakov, D. *et al.* Tailoring emergent spin phenomena in Dirac material heterostructures. *Sci. Adv.* (2018). doi:10.1126/sciadv.aat9349
29. Zollner, K. & Fabian, J. Single and bilayer graphene on topological insulator Bi₂S₃: electronic and spin-orbit properties from first-principles. *arXiv Prepr. arXiv1907.03494* (2019).

30. Zhang, J., Triola, C. & Rossi, E. Proximity effect in graphene-topological-insulator heterostructures. *Phys. Rev. Lett.* **112**, 1–5 (2014).
31. Khokhriakov, D., Karpiak, B., Hoque, A. M. & Dash, S. P. Two-Dimensional Spintronic Circuit Architectures on Large Scale Graphene. *arXiv Prepr. arXiv1905.04151* (2019).
32. Meyer, S. *et al.* Observation of the spin Nernst effect. *Nat. Mater.* **16**, 977 (2017).
33. Chen, Y. L. *et al.* Experimental Realization of a Three-Dimensional Topological Insulator, Bi₂Te₃. *Science* (80-.). **325**, 178 LP – 181 (2009).
34. Bahramy, M. S. *et al.* Emergent quantum confinement at topological insulator surfaces. *Nat. Commun.* **3**, 1159 (2012).
35. Zhang, H. *et al.* Topological insulators in Bi₂Se₃, Bi₂Te₃ and Sb₂Te₃ with a single Dirac cone on the surface. *Nat. Phys.* **5**, 438–442 (2009).
36. Moore, J. E. The birth of topological insulators. *Nature* **464**, 194–198 (2010).
37. Benitez, L. A. *et al.* Tunable room-temperature spin galvanic and spin Hall effects in van der Waals heterostructures. *arXiv Prepr. arXiv1908.07868* (2019).
38. Li, L. *et al.* Electrical Control of the Rashba-Edelstein Effect in a Graphene/2H-TaS₂ Van der Waals Heterostructure at Room Temperature. *arXiv Prepr. arXiv1906.10702* (2019).
39. Hoque, A. M., Khokhriakov, D., Karpiak, B. & Dash, S. P. All-electrical creation and control of giant spin-galvanic effect in 1T-MoTe₂/graphene heterostructures at room temperature. *arXiv Prepr. arXiv1908.09367* (2019).

Methods

Device fabrication

The van der Waals heterostructures were prepared using CVD Gr (from Grolltex Inc) on highly doped Si (with a thermally grown 285-nm-thick SiO₂ layer). The BST flakes (single crystals grown from a melt using a high vertical Bridgeman method, acquired from Miracrys) were exfoliated by conventional scotch tape technique and dry-transferred on top of Gr inside a glovebox. The exfoliation and heterostructure preparation in a controlled N₂ environment is expected to provide higher quality Gr-TI interfaces. Next, appropriate 90-140 nm-thick TI flakes were identified by optical microscopy for device fabrication. The Gr and the Gr-TI heterostructure channels were patterned in Hall bar shapes by electron beam lithography (EBL), followed by oxygen plasma etching. The non-magnetic and magnetic contacts were patterned on Gr in two subsequent EBL steps. The Ti/Au contacts were employed as non-magnetic electrodes on the Gr. For the preparation of ferromagnetic contacts, we used electron beam evaporation to deposit 0.6 nm of Ti, followed by *in situ* oxidation in a pure oxygen atmosphere for 10 minutes to form a TiO₂ tunneling barrier layer. Without exposing the device to the ambient atmosphere, in the same chamber, we deposited 90 nm of Co, after which the devices were finalized by liftoff in warm acetone at 65°C. In the final devices, the Co/TiO₂ contacts on Gr act as the source for spin-polarized electrons, the Gr-TI heterostructure region serves as a channel, and the n⁺⁺ Si/SiO₂ is used as a back gate. The FM tunnel contact resistances (R_c), measured in a three-terminal configuration, were around 4-10 kΩ. The field-effect mobility of the Gr channel in proximity with TIs is ~1600 cm² V⁻¹ s⁻¹. To estimate the interface resistance of Gr-BST in the heterostructure, the graphene stripes were first patterned, followed by exfoliation of BST inside the glovebox and evaporation of contacts on both the Gr and BST. The Gr-BST interface resistance is ~ 3 kΩ at zero-bias conditions (see Fig. S3).

Electrical measurements

The spin-galvanic effect measurements were performed in a cryostat with the sample rotation stage and variable magnetic field. The sample was kept in vacuum and at room temperature. In the experiments, a spin injection bias current was applied using a Keithley 6221 current source, and the nonlocal voltage was detected across the Hall bar structure of Gr-BST using a Keithley 2182A nanovoltmeter; the gate voltage was applied with the SiO₂/Si back gate using a Keithley 2400 multimeter.

Data availability

The data that support the findings of this study are available from the corresponding authors on a reasonable request.

Acknowledgments

The authors acknowledge financial support from the EU FlagEra project (funded by Swedish Research Council VR No. 2015-06813), Swedish Research Council VR project grants (No. 2016-03658), European Union's Horizon 2020 research and innovation program under grant agreements no. 696656 and no. 785219 (Graphene Flagship Core 1 and Core 2), Graphene center and the EI Nano program at Chalmers University of Technology. We acknowledge useful discussions with Bing Zhao in our group. We also acknowledge the support from staff at Quantum Device Physics Laboratory and Nanofabrication laboratory at Chalmers University of Technology.

Author affiliations

¹Department of Microtechnology and Nanoscience, Chalmers University of Technology, SE-41296, Göteborg, Sweden

Contributions

SPD and DK conceived the idea and designed the experiments. DK fabricated and characterized the devices. BK and AMH participated in graphene preparation. DK and SPD analyzed and interpreted the experimental data, compiled the figures and wrote the manuscript. SPD supervised the research project.

Competing interests

The authors declare no competing financial interests.

Corresponding authors:

Correspondence and requests for materials should be addressed to Saroj P. Dash, Email: saroj.dash@chalmers.se